International Journal of Innovative Computing, Information and Control
Volume **8**, Number **10(A)**, October **2012**

ICIC International ©2012 ISSN 1349-4198
pp. 6903–6919

FAST ROBUST OBJECT SEGMENTATION BY PROGRESSIVE SHAPE-ANCHOR SELECTING AND ADAPTIVE-THRESHOLDING PIECEWISE LINKING

Din-Yuen Chan[1], Roy C. Hsu[2,*], Tsung-Yi Chiu[1] and Chih-Chuan Lin[1]

[1]Department of Computer Science and Information Engineering
[2]Department of Electrical Engineering
National Chiayi University
No. 300, Syuefu Rd., Chiayi City 60004, Taiwan
*Corresponding author: rchsu@mail.ncyu.edu.tw

Received July 2011; revised April 2012

Abstract. *This paper presents a fast robust object segmentation method for segmenting the target object from a noisy image. First, an anchor-node identification process is employed to select the representative nodes on object's boundaries as shaping anchor nodes (SANs) by performing a boundary-point detecting-sifting (BPDS) on SAN-based scan-lines. Then, an adaptive-thresholding piecewise linking process, named SAN-based piecewise shape linking (SPSL), is used to render a closed contour passing every SAN for getting a precise profile for the image object targeted. When linking of the closed contour fails for some SANs near weak-edge object boundary, the resultant disconnections can be recovered by simply iterative refinement linking. Experiment results demonstrate that the proposed method achieves more accurate object shape detection than other conventional methods in noisy images under different light projections, while the required process cost is not complicated. Such performance mainly comes from the tight cooperation of BPDS and SPSL for the object shape detection task. Consequentially, the proposed object-segmentation method is drastically fast to offer proper object segmentation in noisy images.*

Keywords: Polygon, Shape detection, Object segmentation, Boundary tracking

1. **Introduction.** Rapidly segmenting targeted semantic objects in images with various cluttered backgrounds is a significant and critical stage in raising the application level of image processing. In the early time, Kass et al. proposed the snake model [1], which is a pioneer work in tracking the object boundary by exploiting the deformable active closed curve. Yuen et al. [2] exploited the gradient detection using radiating scan lines with fixed-angle from the estimated image center to detect the location of object border. Thus, snaxel initialization can be automatically made up. This way, however, is not suited to the image with targeted object having irregular inner structured shapes under noisy background, where the image center may not be in the object body. So, some kernel-based parametric active contour models were proposed to overcome the interference of noise and background clutter [3]. Recently, some algorithms [4,5] focus on the accuracy of edge detection in the object boundary in noisy images. The method proposed in [4] uses the fuzzy topology to bias the filtered edges for allowing the use of larger gradient kernel, making the derivative computation less sensitive to noises. Other machine learning based approaches such as HMM [6], FCM [7], and neural network [8], were also proposed for image segmentation; however, their computations are often time-consuming and complex offline-learning parameters were required. Hence, most of the above-mentioned methods

will not be suitable for efficient or online demand in large-scale image processing applications. The multi-segment algorithm [5] can drop the false detection resulted by noises via checking the defined false alarm associated with the probability of gradients aligned with a segment. For extracting the contour of object, the thresholding, the histogram analysis, and the linking are frequently considered as basic units unified in obtaining a systematical solution in image segmentation [9-11]. Based on a traditional algorithm [12], the work in [13] proposed a sufficient combination of threshold segmentation and sequential edge linking to extract the region of interest (ROI). Wang et al. [14] addressed a graph-theoretic algorithm to obtain the perceptually-salient closed border contour by completing the reductions about the setting of solid edge, detecting of alternate cycles, and finding of minimum weight perfect matching [15-18]. However, nowadays, the speed and the robustness to rapidly, automatically segment semantic objects out of noisy images are much more issued. In this study, an efficient robust object-shape detection/segmentation processing having high accuracies is proposed using BPDS and SPSL. Therefore, the segmentation processing to efficiently highlight the shape of targeted object can be treated as necessary and effective pre-processing in significant large-scale signal-processing systems such as content-based image database [22], object-shape classification [23], special medical image [24], and highly-growing emerging 2D-to-3D video conversion [25] systems. In [22], authors addressed a useful specific-purpose fuzzy retrieval system for a variety of car shapes. The work in [23] addressed a neural-network based shape decision framework. In the study [24], the authors aim to measure deformation fields for specified biological tissues from non-rigid objects in MR images. Observing many existing image systems, to adopt an appropriate efficient segmentation mechanism such as our proposed one, which comprises BPDS and SPSL, thereafter, abbreviated as BPSL, does capably highly maintain or even promote the performance of subsequent applied/developed processes. The BPDS can hierarchically and progressively collect an appropriated group of SANs. With SANs on hands, BPSL performs SPSL to rapidly acquire a closed-contour with proper object-boundary matching. Particularly, the threshold of high-pass filtered pixels can automatically accommodate itself to the local circumstance around the pair of currently selected SANs, by which SPSL links a piece of targeted object contour. Thus, such an adaptive process is very naturally focused on the varying localized scope. The remainder of the paper is organized as follows. Section 2 presents the details of BPDS and SPSL for BPSL, where an extended approach with regular implementation, an advanced BPSL, is illustrated for coping with the possible complicated cases. Section 3 provides the simulation results, while concluding remarks are given in Section 4.

2. **The Proposed Method.** The first stage of BPSL, BPDS, requires an initial user-defined rectangle with simple mouse-dragging to roughly cover the area of target object. Generation of such a rectangle is the only interaction related to the user. Within the rectangle, SANs are searched and then linked to form an initial polygonal snake contour to efficiently approximate the object-contour edges of interest. By progressively embedding the single-backup in each of hierarchical stages, which will be detailed later, false-positives and -negatives of selecting the linked nodes to accomplish the object-contour following can be effectively suppressed. Because the uncertainties between desired features and undesired ones always exist in a variety of images, stable, flexible and efficient initialization will be preferred and more applicable for other segmentation tools such as snakes. Hence, the BPDS processing is to rapidly estimate limited shape representative positions emerging likely boundary edge strengths on selective scanning lines. By definition, the nodes at those positions, i.e., SANs, are the specific starting points for further contour segmentation processing, such as the initial snaxels in snakes. The BPDS implementation

comes from the concise postulation: For a line scanning through the object, the variation of average edge strength across the object border (a boundary between two heterogeneous regions, e.g., target object and background) shall be relatively distinguishable than that across the inner of the same region. And, the edge strength of object border pixel is larger than that of its neighboring pixels or the pixel of similar property observed.

The second stage of BPSL, the SPSL processing, is to accomplish the one-pixel boundary curve extraction. With the SANs collected by BPDS, the possible contour representative nodes, the SPSL processing proceeds to link the object contour piece-by-piece, where each resultant curve segment between two adjacent SANs is regarded as a "linking piece". The SPSL contains a linked-node selection rule (LNSR) as well as three operations: adaptive-thresholding, thinning, and directional region growing (DRG) to progressively link and tailor each curve segment of the object shape. Particularly, most edge detection algorithms associated with specific high-pass filtering will in effect encounter a critical problem of determining suitable or relatively precise thresholds to verify "edge" pixels on two occluded object's boundaries. In our adaptive-thresholding, the filtered high-pass outcomes of two adjacent SANs can provide significant references to set the threshold appropriated to the pixels within an area bounded by these two SANs. Thus, the threshold applied to the amplitudes of high-pass filtered pixels can automatically adapt according to the varying local characteristics along tracking the object border. Then, by thinning and DRG, one-pixel-width contour of targeted object can be revealed within a given area. For faithfully recovering the disconnections possibly occurring on the output contour while adopting the prototype BPSL, an iterative refinement linking proposed herein can be further incorporated into BPSL as an advanced BPSL approach to precisely extract the object contour. The procedures of BPDS and SPSL are individually described as the following.

2.1. **The BPDS procedure.** The BPDS is a hierarchical and progressive procedure from the analysis-unit level up to the scan-line level, as shown in Figure 1. The routine of entire BPDS is depicted as follows.

Part 1. Composing the analysis units for the SANs acquisition. The initialization of the edge analysis unit in terms of specific line fragments is composed by the following two steps.

Step 1: *A user-defined rectangle is first selected to approximately cover the target object, and a downsized rectangle is obtained by progressively trimming along its rims and by iteratively checking the differences of quantized chrominance/luminance strengths nearby the renewed rims. The downsized rectangle is then equally divided into four quadrants.*

Step 2: *Each quadrant is individually scanned with horizontal and vertical scan lines of even distance gaps. The fragments generated by those mutually orthogonal lines on a scanning line are defined as the units (U) of this scanning line.*

Generally speaking, to entirely and automatically range a proper area bounding the desired object for segmentation is hard. Hence, in Step 1, the initial user-defined rectangle is a roughly hand-selected (hand-marked) one. The trimming to obtain an initial rectangle having higher object approximation can directly alleviate the background interferences in the contour segmentation/extraction process. The proposed initialization is semi-automatic with only a little aid from user interaction to make the analysis of targeted object be effectively localized and bounded.

Part 2. Selecting edge-representative pixels in two levels. The selection of edge-representative pixels is hierarchically, progressively performed by two-levels, given by:

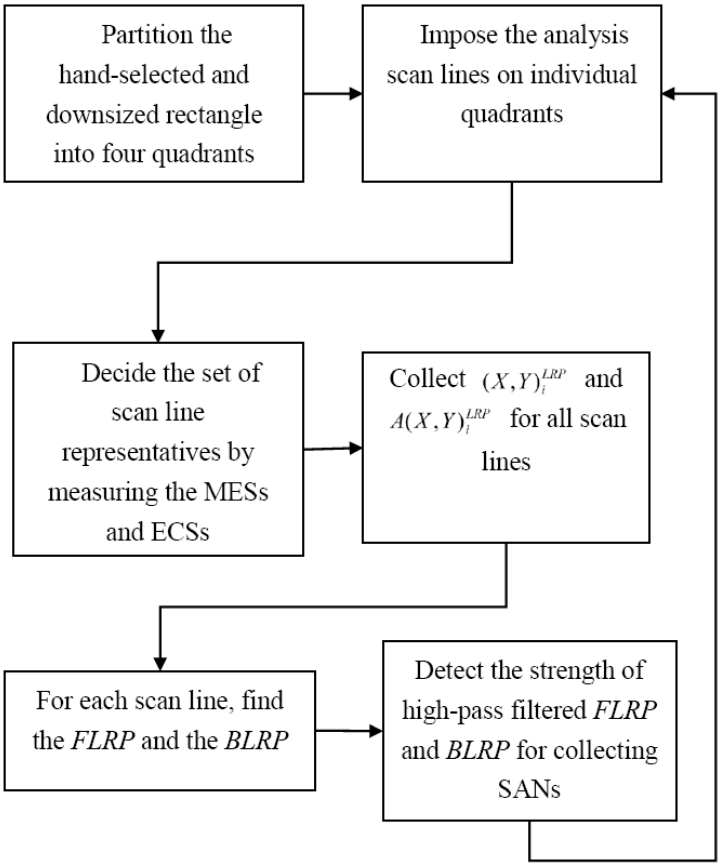

FIGURE 1. Flowchart of BPDS

Step 1: *<the first level selection> On each unit (fragmented piece) along scan-line, find a unit-representative pixel (URP), which has the maximal edge-strength*[1] *(MES), and obtain the edge contrast strength (ECS) of this MES by the calibration of edge-strength mean (ESM) in this scan-line unit. The URP and ECS are obtained for all units along the scan line (l). Assume that* $I(x,y)$ *is the gray-level of the pixel at* (x,y)*, and* $G(x,y)$ *expresses the high-pass result by the Sobel filter at coordinate* (x,y)*, whose amplitude expressed by* $|G(x,y)|$*, is used to measure the edge strength at* (x,y)*. The MES, the URP, and the ECS can then, respectively, be represented by*

$$MES = \max_{(x,y)\in U} |G(x,y)|, \tag{1}$$

$$URP = \{(x,y)||G(x,y)| = MES\}, \text{ and} \tag{2}$$

$$ECS = MES - ESM, \tag{3}$$

where $ESM = \sum_{\forall(x,y)\in U} |G(x,y)|/N$*, and* N *is the number of pixels within each unit* U*.*

Step 2: *<the second level selection> Among the URPs of one scanning line, look for four line-representative pixels (LRPs). The first LRP has the largest edge strength, and the second LRP is the first's "backup" having the second largest edge strength. Again, search another type of LRP, where the third LRP has the largest ECS, and the fourth LPR is the third's "backup" having the second largest ECS. For the ith scan line, the coordinates and the edge strengths, respectively, of its four LRPs constitute the URP-characteristic sets as*

[1]The edge-strength could be evaluated by a widely-used edge detector such as Sobel operator in this work.

given by

$$(X,Y)_i^{LRP} \equiv \{(x,y)LRP(i,j), j = 0,1,2,3\}, \text{ and} \tag{4}$$

$$A(X,Y)_i^{LRP} \equiv \{|G(x,y)LRP(i,j)|, j = 0,1,2,3\}, \tag{5}$$

where $LRP(i,j)$ is the jth URP in the ith scan line.

Part 3. Determining SANs on scan lines. The SANs are regarded as the edge seed points, which play the roles of sourcing nodes for linking the object boundary. The acquisition procedure of SANs is described as follows.

Step 1: *Among the four LRPs of each scan line, the pixel having the maximum absolute x (or y) coordinate for the horizontal (or vertical) scan line is selected as the first-priority line-representative pixel (FLRP). Then, a second-priority (the backup of FLRP) line-representative pixel (BLRP) is set, which has the largest among all summations obtained by adding the edge strength and the contrast strength together for other remaining three LRPs, herein, whose locations need not be further considered.*

Step 2: *For every scanning line, examine whether the FLRP is located nearly on an edge by comparing its detected-edge strength with a pre-determined threshold value, T_{edge}, and if it is, the FLRP is nominated as a SAN. When the FLRP is identified not a close edge pixel, the same test is then operated on its backup, the BLRP, as well. If the BLRP passes the test, it will be considered as a SAN in substituting of the FLRP. Otherwise, no SAN is found in this scan line to support the initial contour position. Specifically, the condition of pixel to meet the SAN requirement is given by*

$$SAN \in \{(x,y)|\, |G(x,y)_{FLRP}| > T_{edge} \text{ or } |G(x,y)_{BLRP}| > T_{edge} > |G(x,y)_{FLRP}|\} \tag{6}$$

It is noted that Part 2 and Part 3 mentioned above are performed one quadrant by one quadrant. After performing the above steps, the set of SANs is obtained by (5) that these SANs are treated as the candidates of nodes identifying the object border.

2.2. **The SPSL procedure.** Without performing additional analyses of local image contents about color, grey-level and texture contrast around each linking SAN, the transversal-cut crossing the narrow zone of targeted object, making the resultant object profile be truncated, will likely happen in linking those nodes, i.e., SANs, for a closed contour. Hence, for simply avoiding the transverse cut (jump) across the object in exhibiting defective object shapes, LNSR with two constraints in SPSL for capturing the actually suitable linking nodes from SANs is proposed as follows.

<**Constraint-1**> *Linking of the SANs will comply with the order of quadrants. So the linking is not allowed to skip the next indexed quadrant when it progresses up to the boundary of current quadrant unless the next indexed quadrant has no any SAN. In practice, in searching the next anchor node near the border of the ith and $(i+1)$th quadrants, the SAN in the $(i+1)$th quadrant adjacent to last SAN in the ith quadrant shall be covered first without considering the SANs of the $(i+2)$th and the $(i+3)$th quadrants.*

<**Constraint-2**> *If the x-coordinate (or y-coordinate) of current linking quadrant is smaller (larger) than that of its next indexed quadrant, the linking of current SAN will obey the rule of monotonic x-coordinates (or y-coordinate) increasing (decreasing) to search the next SAN with the shortest horizontal (or vertical) distance to current SAN. Concurrently, searching the next SAN need not care about if the change of y-coordinates (or x-coordinates) is positive or not.*

Constraint-1 is illustrated by Figure 2, where the "m" SAN is linked to the "n" SAN rather than the "k" SAN as the required linking direction is counterclockwise, although the latter has a very short distance to the "m" SAN.

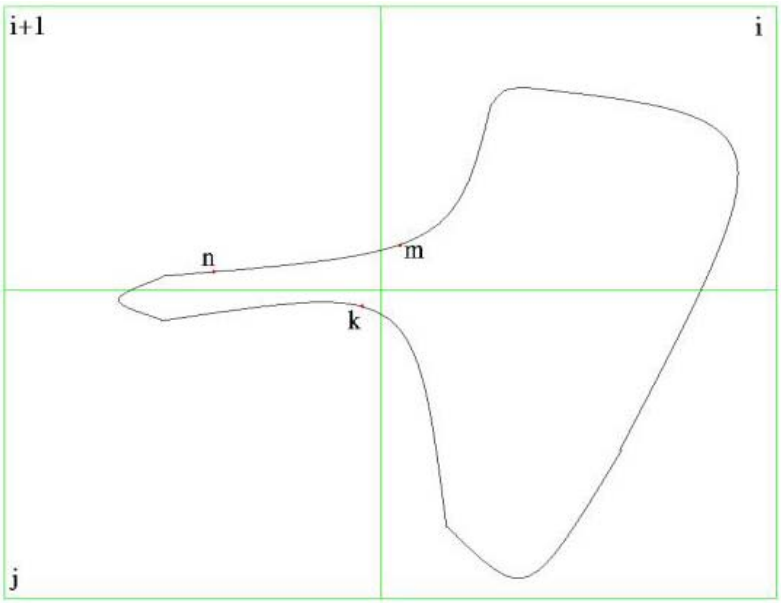

FIGURE 2. The linking of three given SANs under Constraint-1 of SPSL

Hence, Constraint-1 supports a simple yet effective means to segment the targeted object without truncation of object's portion. With the direct linking of SANs by above two rules, a closed polygon can be obtained as one immediate approximation of targeted object shape. The polygon could be linearly inflated from its center to become an initial snake contour to start *snakes* evolution. By such initialization, one can effectively alleviate the possibilities of initial snaxels falling within the targeted object and simultaneously facilitate the rapid convergence of snake contour to the object border. In this study, without performing any additional active model evolution, the latter of SPSL straightforward achieves a perceptually nature contour for representing the object shape. The flowchart of SPSL in acquiring one-pixel-width representative boundary curve is shown by Figure 3. With SANs on hand, SPSL performs detection and linking of the object contour fragment by fragment to obtain a one-pixel-width representative boundary of the object. The SPSL processing mainly includes adaptive-threshold truncation, thinning, and directional region growing, which is shown as follows.

Step 1: *Set either clockwise or counterclockwise direction as the tracking direction. And then pick a SAN, whose x (or y) coordinate is the maximal/minimal, as a piecewise-linking start point (PLSP).*

Step 2: *Along the tracking direction, search the SAN closest to PLSP as the piecewise-linking end point (PLEP). Exploit the current PLSP and PLEP as the diagonal corners of a rectangular mask in covering the pixels between them. And then, perform high-pass filtering using the Sobel filter throughout the pixels within this mask.*

Step 3: *An adaptive threshold is set as the distance-dependent weighting sum of high-pass filtered results of the PLSP and PLEP. The adaptive weights are inversely proportion to the distances of the two terminal points, the PLSP and the PLEP. Through truncation by thresholding, the filtered grey-level* $p_{filtered}(x, y)$ *at* (x, y) *lying between the PLSP and the PLEP, whose high-pass filtered results are* $p_{filtered}(x_s, y_s)$ *and* $p_{filtered}(x_e, y_e)$*, respectively, becomes* $p'_{filtered}(x, y)$ *by*

$$p'_{filtered}(x,y) = \begin{cases} 1, \text{ if } p_{filtered}(x,y) \geq \omega p_{filtered}(x_s,y_s) + (1-\omega)p_{filtered}(x_e,y_e) - \delta \\ 0, \text{ otherwise} \end{cases}, \quad (7)$$

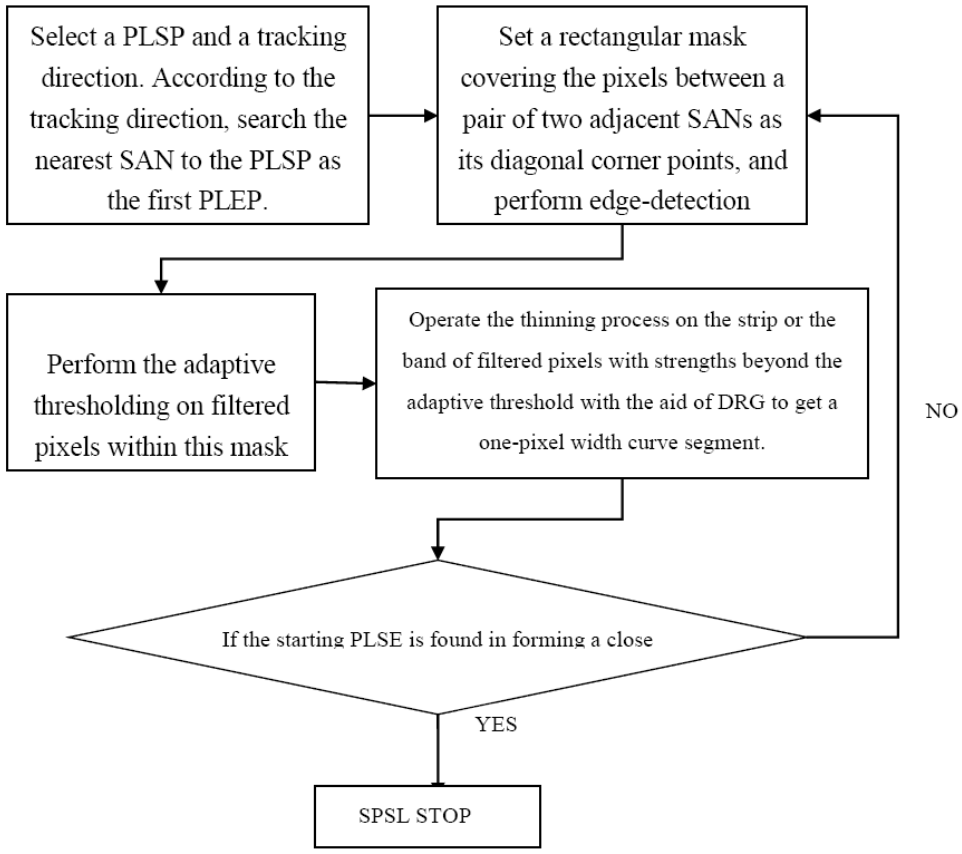

FIGURE 3. Flowchart of the SPSL processing

where $p'_{filtered}(x,y) = 1$ *indicates that the position* (x,y) *is a contour candidate,* $\omega = \frac{\sqrt{(x-x_e)^2+(y-y_e)^2}}{\sqrt{(x-x_s)^2+(y-y_s)^2}+\sqrt{(x-x_e)^2+(y-y_e)^2}}$, *and* δ *is an empirical value associated with the standard deviation of filtered SAN grey levels.*

Step 4: *Perform the thinning processing [21] on all contour candidates in the rectangular mask with corners specified by currently paired PLSP and PLEP. If a one-pixel width curve with terminals points, i.e., current PLSP and PLEP, can be directly obtained, the SPSL proceeds to Step 5. Otherwise, the one-pixel width segment connection will be performed by DRG from the breaking point of the curve stretched by current PLSP to that by current PLEP.*

Step 5: *If the current PLEP equals or adequately approximates the first PLSP, the SPSL stops. Otherwise, let the current PLEP act as the new PLSP and the SPSL proceeds to Step 2 to build the next object-contour segment.*

In (7), $\omega p_{filtered}(x_s,y_s) + (1-\omega)p_{filtered}(x_e,y_e)$ is a complementary sum, where ω is naturally adaptive according to the distances from the PLSP and the PLEP. In Step 4, because the PLEP is kept as the aim in every rectangular mask with diagonal corners of PLSP and PLEP pair, by DRG, the region growing to link two close breaking fragments can be easily obtained under an easy direction control. Unlike traditional region growing, the DRG processing merely has to determine the nearest one from three neighboring points in the direction of the PLEP among the 8-connectivity neighbors of the current linking node as the next linking node. The selection of three neighboring points from 8-connectivity points will depend on the relative orientation (the located quadrant) of the target point vs. the current linking (the referred origin) node so that the three points are

limited as one of 4 corners in the 3×3 block centered at the current linking node. Thus, by the directional pixel growing, the connection of breaking curves in a limited area (between PLSP and PLEP), where the edges may be strength-inconsistent, inadequate, or messy, is efficient. Therefore, with the effect of adaptive thresholding in Step 3, progressively connecting object-contour segments for a representative one-pixel-width object profile can be easily completed without taking care of possible troublesome branching.

2.3. **Extension to an advanced SPSL approach for complicated cases.** Because the abovementioned SPSL is a one-pass linking processing, linking partial pairs of PLSPs and PLEPs might not be successful for complicated cases, for example, that the target surface has high complex variations or non-uniform light projections. So, if necessary, the SPSL need to be extended as an advanced BSPL, abbreviated hereafter as ABSPL, to solve this problem. The ABSPL procedure can be easily attained by straightforwardly modifying BPSL as a BPSL approach of recursive type with a regular structure. The ABSPL proposed herein is a multi-pass recursive algorithm depicted by two stages as below.

<**Stage 1**> *After SPSL, the localized focus regions covering every two disconnected SANs in the pieces of extracted contour are re-scanned with higher scan-line resolutions. In a focus region, by performing BPDS, two new modified SANs are then found to replace the pair of the unsuccessfully-linking SANs in the previous pass, and the higher-resolution SANs between the above two SANs are also yielded.*

<**Stage 2**> *Operate SPSL on the new SANs to connect every disconnected piece. Check whether there are still disconnected pieces or not in the extracted contour. If it does, go to Stage 1 to perform the next pass of ABSPL once-more in contracted focus regions. Otherwise, a closed contour achieved by ABSPL is identified for representing the shape of target object.*

Because the refinement in ABSPL is localized and its iteration is hierarchical based on fast increased scan-line resolution of SPSL, the incurred computational cost relative to BPSL is very limited yet can be traded for a rather trustworthy performance gain. In short, ABSPL can efficiently correct the partial errors and raise the precision for the segmented outcome resulting from BPSL.

2.4. **Discussions.** For simplicity, the contour representative (initial boundary) SANs, which are obtained by the BPDS with LNSR-based selection, can be directly linked up to acquire a polygon to approximate or characterize the object profile. Alternatively, the precision (accuracy) increase of image segmentation can be traded with the computational speed for making the results of BPSL less conservative. Herein, we enumerate two approaches. The first approach is to modify the original scheme "BPDS + SSPL" as "BPDS + (texture-dependent SSPL)", and the second is "BPDS with (LNSR-based selection) + snakes". The former additionally includes an online verge-texture judgment along SSPL to drop the weak SAN candidates. In the latter approach, the processing of BPDS with LNSR-based selection, plays the role of automatically picking up initial snaxels for performing *Snakes* [1,19], within a given target zone. This can enable the evolving snake contour be more promptly and accurately converged over traditional snakes [1] without specific initialization. In short, due to the high convenience of modification or combination-variation for specified improvements, our proposed scheme, BPDS + SSPL, could be considered as a new basic image-processing function just like "*opening*" and "*closing*" morphological functions for object contour segmentation.

3. **Experimental Results.** Here are the experimental results of this study.

3.1. **The results of initial boundary SANs obtained by BPDS + (LNSR-based selection).** In this study, four artificial images, which are two round object image with different levels of noise, a U-shape object image with noise, and the blurred image of the noisy round object image, are created and shown in Figure 4(a), Figure 4(b), Figure 4(c), and Figure 4(d), respectively, to first evaluate the performance of BPDS + (LNSR-based selection). The nodes obtained by the BPDS + (LNSR-based selection) can be simply connected as a approximated object-profile polygon, which could be further processed by either snake evolution or the SPSL. So, they are named initial boundary SANs or contour representative SANs. Because the position of true edge points are known when the artificial images of round object and U-shape object are created, these images can be used to test the accuracy and error rate of the SANs selected by BPDS and the contour extracted by the SPSL. To test the robustness and effectiveness of the proposed method

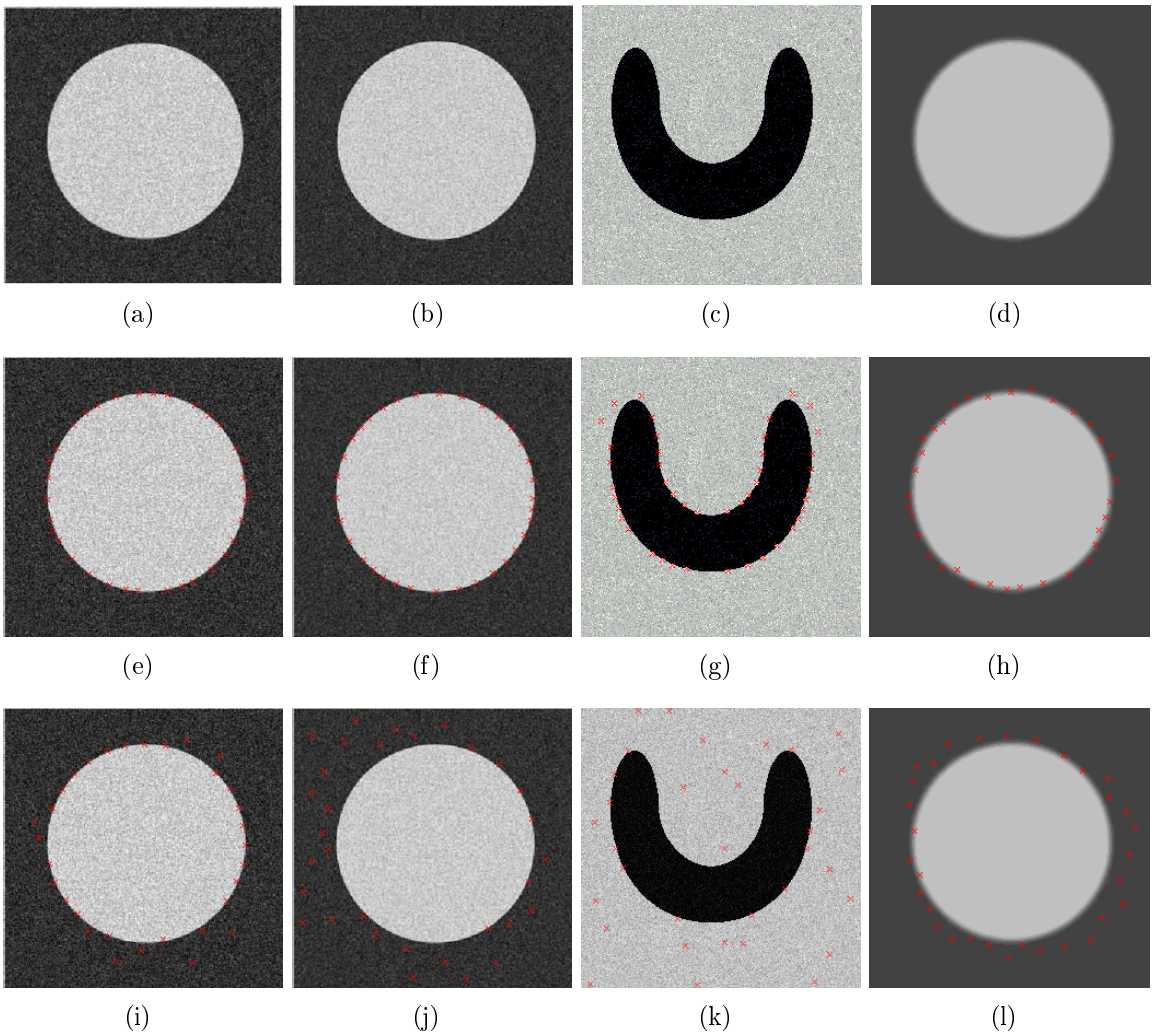

FIGURE 4. Experimental results of SAN selection by the BPDS and snaxel imitialization of the method of Yuen et al. Artificial images of a round object with noise (a) SNR = 23.8dB and (b) 20.3dB, (c) a U-shape object with noise, and (d) a blurred image of the noisy image in (b). Figures 4(e)-4(h) are the BPDS results of the image in (a), (b), (c), and (d), respectively. Figures 4(i)-4(l) are the results of the method of Yuen et al. for the image in Figures 4(a)-4(d), respectively.

under noise influence, different levels of zero mean white Gaussian noise are added to the original artificial images of the round and U-shape object as,

$$I_n = I_o + N(0, \sigma), \tag{8}$$

where I_o is the original image, $N(0, \sigma)$ is a White Gaussian noise with zero mean and variance σ, and I_n is the noise-corrupted image. The signal-to-noise ratio of the noisy images of Figrue 4(a), Figure 4(b), and Figure 4(c) is 23.9dB, 20.3dB, and 20.3dB, respectively. The blurred image of round object in Figure 4(d) is created by smoothing the noisy round object image of Figrue 4(b) with a 3×3 window, which is used to evaluate how well the proposed method can find out the initial snaxels and exact contour for image under blurred effect. The experimental results of SAN selection by the first stage of BSPL, the BPDS, are compared with the method of Yuen et al. [2]. In the method of Yuen et al., the center of gravity of the tested image is first computed and scan lines, whose number is in power of 2, with equal degrees are emitted from the center of gravity to search the most distant point with the largest high-pass filtered magnitude, i.e., the candidate initial snaxel, along the scan line. Figures 4(e)-4(h), respectively, show the BPDS results of the round object image with noise SNR = 23.9dB in Figure 4(a) and SNR = 20.3dB in Figure 4(b), the U-shape object image with noise SNR = 20.3dB in Figure 4(c), and the blurred image of the noisy round object image of Figure 4(b) in Figure 4(c), while Figures 4(i), 4(j), 4(k), and 4(l), respectively, show the snaxel initialization results of Yuen's method for the images in Figures 4(a)-4(d). Visual inspection shows that most of the SANs found by BPDS for four test images are fitted to the curvature and distance of the artificial image's contour which constitutes a better definition of contour pixel initialization than the method of Yuen et al., where some false initialization of contour pixels are obtained and spread far off the boundary of the test images.

To quantitatively compare the accuracy of BPDS and the method of Yuen et al., the true positive, which is defined as the ratio of true detected initial boundary pixels to total detected initial boundary pixels, is used as the comparing parameter and Table 1 shows the results.

According to Table 1, the BPDS obtained better accuracy in selecting initial boundary pixels than the method of Yuen et al., for all four artificial images. The BPDS significantly outperforms the comparing method especially for the artificial noisy U-shape object image. This can be understood that our proposed BPDS method searches possible SANs

TABLE 1. Accuracy comparison of the BPDS and the method of Yuen et al. of the initial boundary pixel selection in terms of true positive, i.e., true detected initial boundary pixels/total detected initial boundary pixels

Method / **Image**	**The BPDS**	**Method of Yuen et al.**
A round object image with noise, SNR = 23.9dB	30/34 = 88.2%	22/32 = 68.7%
A round object image with noise, SNR = 20.3dB	28/34 = 79.4%	19/32 = 59.3%
A U-shape object image with noise, SNR = 20.3dB	28/34 = 82.3%	11/32 = 34%
The blurred image of the noisy round object image with SNR = 20.3dB	25/34 = 73.5%	8/32 = 25%

TABLE 2. Statistical comparison of the initial boundary pixels selected by the BPDS and method of Yuen et al. in terms of mean distance and standard deviation between each pair of selected neighboring boundary pixels

Method / Images	BPDS		Method of Yuen et al.	
Parameter	$\overline{d}$	σ	$\overline{d}$	σ
A round object image with noise, SNR = 23.9dB	15.24	3.26	21.08	5.12
A round object image with noise, SNR = 20.3dB	16.7	3.63	27.14	6.57
A U-shape object image with noise, SNR = 20.3dB	21.86	8.92	39.67	21.25
The blurred image of the noisy round object image with SNR = 20.3dB	17.31	4.21	21.13	4.19

within each unit along both horizontal and vertical scan-lines with the weak edge evidence screening and supporting such that the initial boundary pixels can be robustly detected even for object of irregular shape with noise. On the other hand, the method of Yuen et al. first computes the CoG of image and then searches the initial snaxels along the scan-lines emitting from the CoG such that it might fail to detected some boundary pixels when the CoG is not inside the object for object with irregular shape and deep concavities, such as the U-shape object. To evaluate the relative locations of initial boundary pixels selected by the BPDS and the method of Yuen et al., and further evaluate their influence on the convergence of snake, mean distances, $\overline{d}$, and standard deviation, σ, between each neighboring initial boundary pixels are computed as shown in Table 2 for four artificial images. The values of mean distance and standard deviation of each pair of neighboring boundary pixels selected by the BPDS are far smaller than these of the method of Yuen et al., which indicates that the initial boundary pixels selected by BPDS are evenly and closely located around the boundary of the object. By inspecting Figure 4 and Table 1, and Table 2, one can find that Yuen et al. method searches farthest edge pixels along each angle-fixed scan-line; hence it lacks flexibility and is easily affected by noise. The BPDS on the contrary finds the initial boundary pixels by searching the scan-lines along both the horizontal and the vertical direction with a hierarchical screening and supporting concept, which leads to better accuracy in selecting initial boundary pixels.

To further demonstrate the influence of the set of initial boundary pixels, selected by the BPDS and by the method of Yuen et al., in obtaining a closed object contour, the initialization results are further utilized for running snake. In executing snake, the locations of initial boundary pixels are gradually changed and controlled to close to the object contour; therefore the closer the selected initial boundary pixels are to the real object contour, the faster the snake converges and the higher the precision for the closed contour extracted with respect to the object's real contours. The extracted contour of snake utilized the initial boundary pixels, i.e., SANs, selected by BPDS and the method of Yuen et al. for the four artificial images as shown in Figure 5. The first and second rows of Figure 5, respectively, show the snake results utilizing the initial boundary pixels obtained by the BPDS and the method of Yuen et al. for the four artificial images.

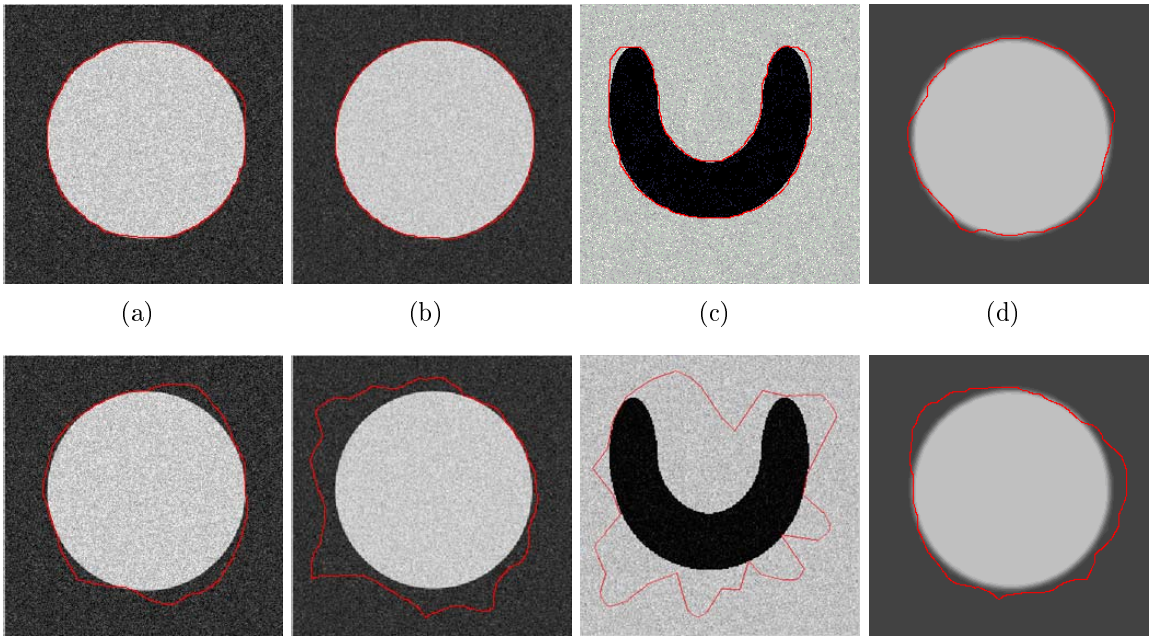

FIGURE 5. Snake result of four artificial images using initial snaxels selected by BPDS and by the method of Yuen et al. Snake results of noisy round object image with SNR = 23.9dB (a) and 20.3dB (b), noisy U-shape object image (c), and the blurred noisy round object image (d) using BPDS selected SANs. Snake results of noisy round object image with SNR = 23.9dB (e) and 20.3dB (f), noisy U-shape object image (g), and the blurred noisy round object image (h) using initial snaxels selected by the method of Yuen et al.

Experimental results again demonstrate that the object contour extracted by snake for the four artificial object images utilizing the initial boundary pixels, i.e., SANs, selected by BPDS is much closer to the real object's contour than those of the Yuen et al. method because a lot of the initial boundary pixels selected by the method of Yuen et al. are far from the true boundary such that an expanded closed object contour with extrusion is obtained when the snake converges.

To quantitatively compare the influence of the set of initial boundary pixels, selected by different initialization methods, in obtaining a closed object contour by the snake, the false positive is used as the comparing parameter and is defined as the ratio of the number of false detected initial boundary pixels to the number of total detected boundary pixels. The results of false positive of the four comparing methods for the four artificial images are shown in Table 3. According to Table 3, the BPDS have the smallest false positive than the method of Yuen et al. for extracting a contour by running the snake for the four artificial images.

3.2. **SAN-based piecewise shape linking (SPSL) results.** To investigate the accuracy and effectiveness of SPSL for contour linking, experimental results of SPSL, the conventional snake, and two other snake methods (GVF snake [26], NGVF snake [27]) for the four artificial images in Figure 4 are first compared using the same set of initial boundary pixels selected by the BPDS as in Figures 4(e)-4(h). Figure 6 shows the results of contour linking, for the four artificial images by the BPDS and other snake methods.

TABLE 3. False positive of the extracted contours by the snake (i.e., the number of false detected initial boundary pixels/the number of total detected boundary pixels) using initial boundary pixels selected by different methods for the two artificial images

Initialization Method / Image	BPDS	Method of Yuen et al.
A round object image with noise, SNR = 23.9dB	19/564 = 3.36%	337/564 = 59.7%
A round object image with noise, SNR = 20.3dB	21/564 = 3.7%	374/564 = 66.3%
A U-shape object image with noise, SNR = 20.3dB	68/628 = 10.8%	472/628 = 75.1%
The blurred image of the noisy round object image with SNR = 20.3dB	104/564 = 18.4%	395/564 = 70%

The first row of Figure 6, Figures 6(a)-6(d), respectively, demonstrates the contour extracted for the artificial noisy round object image with SNR = 23.9dB, 20.3dB, noisy U-shape object image, and the blurred noisy round object image by the SPSL, while the 2nd, the 3rd, the 4th row of Figure 6, respectively, show the contour linking results of the four artificial images by the conventional snake, GVF snake and the NGVF snake. Experimental results of Figures 6(a)-6(d) exhibit that the SPSL links the real object boundary piece-by-piece in constructing an accurate closed object contour matching to the object's true contour with better precision than other snake's methods with which there are some detected pixels deviating from the true boundary.

Table 4 shows the quantitative comparison in terms of true positive by testing SPSL and different snake methods utilizing the initial boundary pixels selected by the BPDS for the four artificial images. The true positive is defined as the ratio of the number of true detected boundary pixels to the total number of detected boundary pixels. By examining Table 4, the true positives of contour extraction result by SPSL are in comparable with that of NGVF but are $2 \sim 4\%$ better than those of conventional and GVF snake methods. It again demonstrates the advantage of SPSL in integrating the adaptive-thresholding, thinning, and directional region growing for contour linking, which provides more local structure information when compared with snake methods, which relies on energy-minimizing spline guided by internal forces and attracted by external forces in determining contour evolution.

3.3. **BPSL results.** To finally demonstrate the effectiveness and efficiency of the BPSL in contour extraction for real images, the BPSL are applied to several real world images and the extraction results of those real images for are shown in Figure 7. Figure 7(a) and Figure 7(b), respectively, show the image of an skyscraper and a noisy vase image with SNR = 26.4dB, while Figure 7(c) and Figure 7(d), respectively, show the image of two object image from regions of interest in medical image. Figures 7(e)-7(h) shows the results of the proposed BSPL, i.e., BPDS + SPSL, for the four real world images. By examining on the contour extraction results of Figure 7, one can see that the closed object contour of each image is extracted by BPSL. Visual inspection of Figures 7(e)-7(h) again exhibits that BSPL performs well for real images even the image is corrupted with noises.

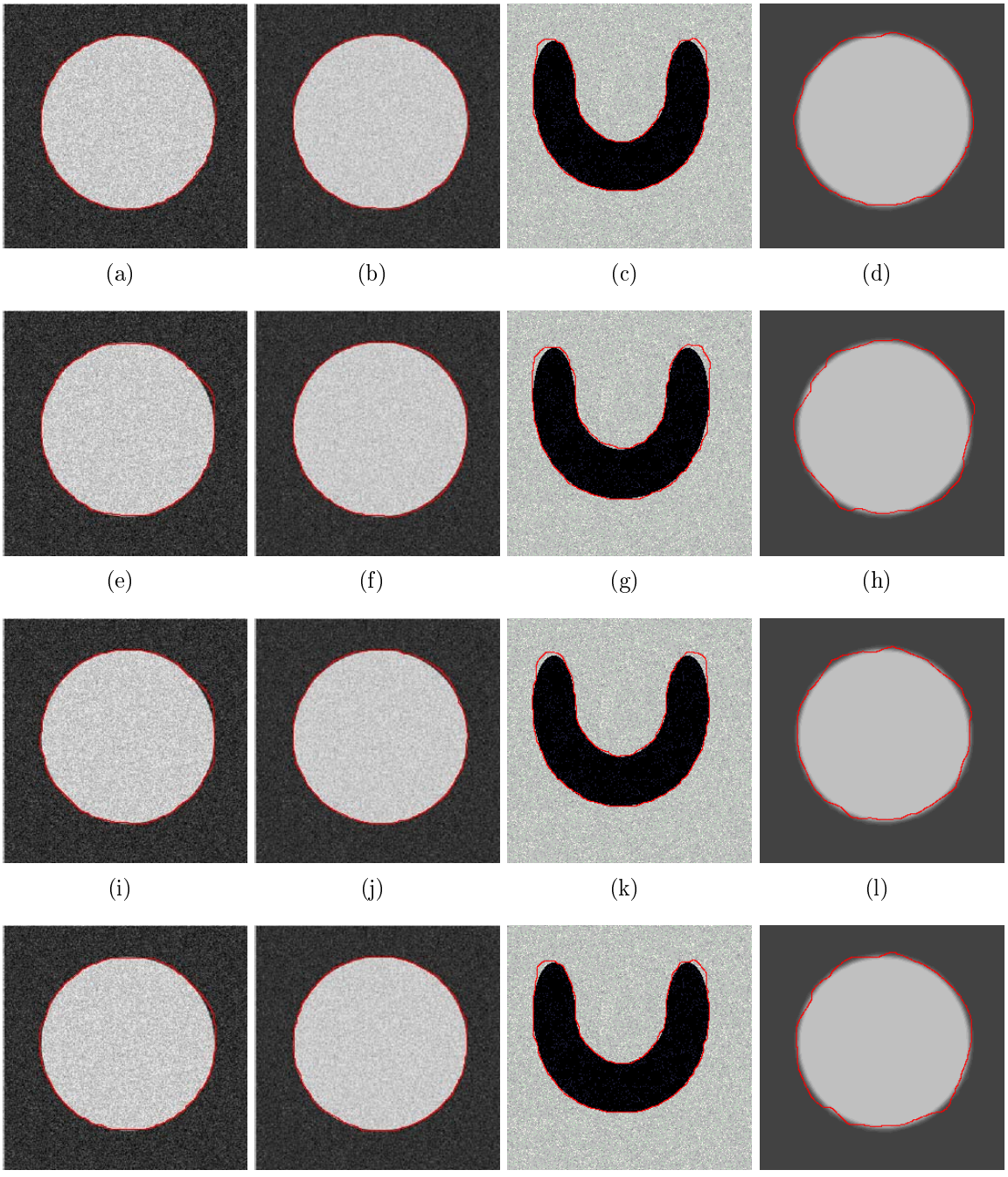

FIGURE 6. Experimental results of SPSL, in comparison with the results of the conventional snake, GVF snake, and NGVF snake for the four artificial images using the same SANs detected by the BPDS in Figures 4(e)-4(h). Figures 6(a)-6(d) the contour linked by SPSL, Figures 6(e)-6(h) the contour obtained by the conventional snake, Figures 6(i)-6(l) the contour obtained by the GVF snake, and Figures 6(m)-6(p) the contour obtained by the NGVF snake.

TABLE 4. Quantitative comparison in terms of true positive (i.e., the number of true detected boundary pixels/the total number of detected boundary pixels) for SPSL and different snake methods utilizing the initial boundary pixels selected by the BPDS for the four artificial images

Method / Image	SPSL	Snake	GVF snake	NGVF snake
Round object (with SNR = 23.9dB)	553/564 = 98.04%	545/564 = 96.63%	547/564 = 96.98%	555/564 = 98.4%
Round object (with SNR = 20.3dB)	550/564 = 97.51%	543/564 = 96.21%	531/564 = 94.14%	547/564 = 96.98%
U-shape Object	572/628 = 91.08%	560/628 = 89.17%	567/628 = 90.28%	576/628 = 91.71%
Blurred round object	481/564 = 85.28%	460/564 = 81.56%	468/564 = 82.97%	475/564 = 84.21%

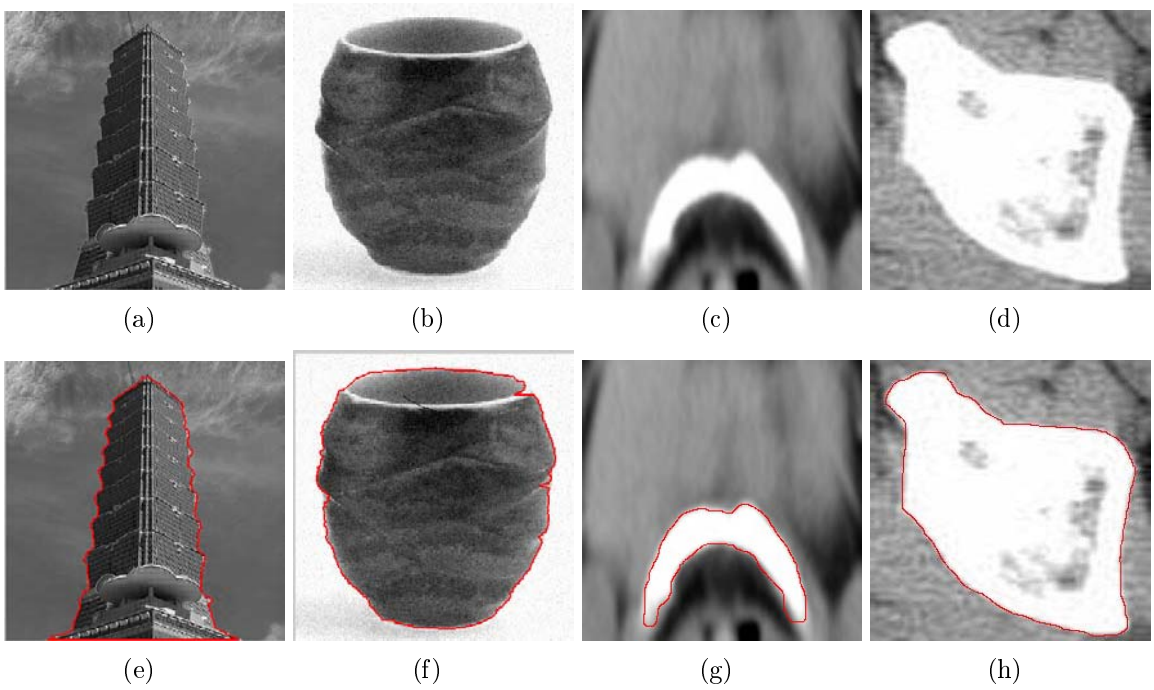

FIGURE 7. (a) A real image of a skyscraper. (b) A noisy vase image with SNR = 26.4dB. (c) medical object image (1), (d) medical object image (2). (e), (f), (g), and (h), respectively, show the contour extraction results for image object in (a), (b), (c), and (d).

4. **Conclusions.** A robust contour extraction method denoted as BPSL is proposed in this study. The BPDS and the SPSL are two main ingredients of BPSL that both methods appear simple yet effective in practical implementation for object contour extraction. Through the BPDS, a polygon given by resulted SANs can be obtained to roughly approximate the profile of a targeted object. The SANs obtained by the BPDS can act as the fixed boundary-tracking points for the SPSL or alternatively as the initial snaxels for the snake processing to further precisely delineate the object shape for a closed object contour. The consecutive integration of the BPDS and the SPSL offers a solid construction in tracking object's boundary. The high-pass filter responses of SANs can provide quite valuable references in the thresholding of edge-detection. Experimental results of the BPDS is compared with that of an existing snake initialization method, which exhibits that under the same corrupted noises, the BPDS finds out better initialization of snaxels

and the SPSL obtains a final closed contour for image object with a higher definition of contour than several snake methods, and most importantly that the BPSL converges faster than the existing methods of snake. Consequentially, the main advantages of the proposed object contour extraction are having low computational complexity and with robustness in accomplishing immediate object-segmentation from noisy images. However, up to now, the popularity of content-based image database is still limited by the speed of identifying object in region of interest (ROI). Hence, the BPSL function could be a quite useful pre-processing apparatus to identify the shape of ROI for multimedia applications. Due to the high regular and concise structure, the BPSL processor is hardware-efficient.

Acknowledgement. The authors would like to thank the National Science Council of Taiwan for partially supporting this work under the projects, NSC 97-2221-E-415-016, NSC97-2221-E-415-017 and NSC 100-2221-E-415-016. This work was also supported in part by the Ministry of Economic Affairs of Taiwan, under Contract 101-EC-17-A-02-S1-201.

REFERENCES

[1] M. Kass, A. Witkin and D. Terzopoulos, Snakes: Active contour models, *International Journal of Computer Vision*, vol.1, no.4, pp.321-331, 1988.

[2] P. C. Yuen, G. C. Feng and J. P. Zhou, A contour detection method: Initialization and contour model, *Pattern Recognition Letters*, vol.20, no.2, pp.141-148, 1999.

[3] C. H. Yang, S. H. Lai and L. W. Chang, Robust face matching under different lighting conditions, *Proc. of the IEEE Conf. on Multimedia and Expo*, vol.2, pp.149-152, 2002.

[4] A. Mishra and A. Wong, KPAC: A kernel-based parametric active contour method for fast image segmentation, *IEEE Trans. on Signal Processing Letters*, vol.17, no.3, pp.312-315, 2010.

[5] H. G. Senel, Topological gradient operator for edge detection, *International Conference on Image Processing*, vol.3, pp.61-64, 2007.

[6] Y. Yu and S. T. Acton, Speckle reducing anisotropic diffusion, *IEEE Transactions on Image Processing*, vol.11, no.11, pp.1260-1270, 2002.

[7] R. Souvenir, J. Kraftchick, S. Lee, M. G. Clemens and M. C. Shin, Cell motion analysis without explicit tracking, *IEEE Transactions on Computer Vision and Pattern Recognition*, pp.1-7, 2008.

[8] T. Y. Zhang and C. Y. Suen, A fast parallel algorithm for thinning digital pattern, *Communications of the ACM*, vol.27, no.3, pp.236-239, 1984.

[9] N. Otsu, A threshold selection method from gray-level histograms, *IEEE Trans. on System, Man, and Cybernetics*, vol.9, no.1, pp.62-66, 1979.

[10] S. Wang, T. Kubota, J. M. Siskind and J. Wang, Salient closed boundary extraction with ratio contour, *IEEE Trans. on Pattern Analysis and Machine Intelligence*, vol.27, no.4, pp.546-560, 2005.

[11] B. Saha, N. Ray and H. Zhang, Snake validation: A PCA-based outlier detection method, *IEEE Signal Processing Letters*, vol.16, no.6, pp.549-552, 2009.

[12] R. G. Gioi, J. Jakubowicz and G. Randall, Multisegment detection, *IEEE Conf. on Image Processing*, vol.2, pp.253-256, 2007.

[13] A. Mishra, A. Wong, W. Zhang, D. Clausi and P. Fieguth, Improved interactive medical image segmentation using enhanced intelligent scissors (eis), *Annu. Int. Conf. IEEE Engineering in Medicine and Biology*, vol.60, no.5, pp.3083-3086, 2008.

[14] X.-Y. Wang and J. Bu, A fast and robust image segmentation using FCM with spatial information, *Digital Signal Processing*, vol.20, no.4, pp.1173-1182, 2010.

[15] Z. Iscan, A. Yuksel, Z. Dokur, M. Korurek and T. Olmez, Medical image segmentation with transform and moment based features and incremental supervised neural network, *Digital Signal Processing*, vol.19, no.5, pp.890-901, 2009.

[16] R. Medina-Carnicer, A. Carmona-Poyato, R. Muñoz-Salinas and F. J. Madrid-cuevas, Determining hysteresis thresholds for edge detection by combining the advantages and disadvantages of thresholding methods, *IEEE Trans. on Image Processing*, vol.19, no.1, pp.165-173, 2010.

[17] X. Shen, C. R. Dietlein, E.Grossman, Z. Popovic and F. G. Meyer, Detection and segmentation of concealed object in terahertz image, *IEEE Trans. on Image Processing*, vol.17, no.12, pp.2465-2475, 2008.

[18] Y. B. Chen, A robust fully automatic scheme for general image segmentation, *Digital Signal Processing*, vol.21, no.1, pp.87-99, 2011.

[19] C. Heinzl, J. Kastner and E. Gröller, Surface extraction from multi-material components for metrology using dual energy CT, *IEEE Transactions on Visualization and Computer Graphics*, vol.13, no.6, pp.1520-1527, 2002.

[20] L. Wei, Z. S. Bin, R. X. Yi and D. Peng, An improved sequential edge linking model for contour detection in medical images, *IEEE Conf. on Industrial Electronics and Applications*, pp.3757-3760, 2009.

[21] R. C. Gonzalez and R. E. Woods, *Digital Image Processing*, 3rd Edition, Prentice Hall, 2007.

[22] T. Samatsu, K. Tachikawa and Y. Shi, Image processing for car shapes in the fuzzy retrieval system, *ICIC Express Letters, Part B: Applications*, vol.1, no.1, pp.1-7, 2010.

[23] L. A. Machowski and T. Marwala, Using an object oriented calculation process framework and neural networks for classification of image shapes, *International Journal of Innovative Computing, Information and Control*, vol.1, no.4, pp.609-623, 2005.

[24] P. Zhang, S. Hirai and K. Endo, A feature matching-based approach to deformation fields measurement from MR images of non-rigid object, *International Journal of Innovative Computing, Information and Control*, vol.6, no.12, pp.107-151, 2008.

[25] R. Sandhu, S. Dambreville, A. Yezzi and A. Tannenbaum, A non-rigid Kernel-based framework for 2D-3D pose estimation and 2D image segmentation, *IEEE Transactions on Pattern Analysis and Machine Intelligence*, vol.33, no.6, pp.1098-1115, 2011.

[26] C. Xu and J. L. Prince, Snakes, shapes, and gradient vector flow, *IEEE Trans. Image Processing*, vol.7, no.3, pp.359-369, 1998.

[27] J. Ning, C. Wu, S. Liu and S. Yang, NGVF: An improved external force field for active contour model, *Pattern Recognition Letters*, vol.28, no.1, pp.58-63, 2007.